Published in final edited form as:
Exp Eye Res. 2013 November ; 0: . doi:10.1016/j.exer.2013.07.023.

Novel Compstatin Family Peptides Inhibit Complement Activation by Drusen-Like Deposits in Human Retinal Pigmented Epithelial Cell Cultures

Ronald D. Gorham Jr[1,#], **David L. Forest**[2,#], **Phanourios Tamamis**[3,#], **Aliana López de Victoria**[1], **Márta Kraszni**[4,+], **Chris A. Kieslich**[1], **Christopher D. Banna**[2], **Meghan L. Bellows-Peterson**[5], **Cynthia K. Larive**[4], **Christodoulos A. Floudas**[5], **Georgios Archontis**[3], **Lincoln V. Johnson**[*,2], and **Dimitrios Morikis**[*,1]

[1]Department of Bioengineering, University of California, Riverside, CA, USA

[2]Center for the Study of Macular Degeneration, Neuroscience Research Institute, University of California, Santa Barbara, CA, USA

[3]Department of Physics, University of Cyprus, Nicosia, Cyprus

[4]Department of Chemistry, University of California, Riverside, CA, 92521, USA

[5]Department of Chemical and Biological Engineering, Princeton University, Princeton, NJ, USA

Abstract

We have used a novel human retinal pigmented epithelial (RPE) cell-based model that mimics drusen biogenesis and the pathobiology of age-related macular degeneration to evaluate the efficacy of newly designed peptide inhibitors of the complement system. The peptides belong to the compstatin family and, compared to existing compstatin analogs, have been optimized to promote binding to their target, complement protein C3, and to enhance solubility by improving their polarity/hydrophobicity ratios. Based on analysis of molecular dynamics simulation data of peptide-C3 complexes, novel binding features were designed by introducing intermolecular salt bridge-forming arginines at the N-terminus and at position -1 of N-terminal dipeptide extensions. Our study demonstrates that the RPE cell assay has discriminatory capability for measuring the efficacy and potency of inhibitory peptides in a macular disease environment.

Keywords

macular degeneration; drusen; retinal pigmented epithelium; complement system; complement inhibitors; compstatin family peptides; molecular dynamics

[*]**Corresponding Authors**: Lincoln V. Johnson, Center for the Study of Macular Degeneration, Neuroscience Research Institute, University of California, Santa Barbara, CA 93106; l_johnso@lifesci.ucsb.edu; Tel.: 805-893-2965. Dimitrios Morikis, Department of Bioengineering, University of California, Riverside, CA, 92521; dmorikis@ucr.edu; Tel.: 951-827-2696.
[#]These authors contributed equally to the work
[+]**Permanent Address**: Department of Pharmaceutical Chemistry, Semmelweis University, Budapest, Hungary

1. Introduction

Drusen are extracellular deposits that are a hallmark of age-related macular degeneration (AMD) and a risk factor for advanced AMD pathology (CAPT, 2008; Klein et al., 2008; Rudolf et al., 2008). These deposits form between the basal surface of the retinal pigmented epithelium (RPE) and Bruch's membrane and have been linked to the activation of the complement system and associated inflammatory processes that contribute to AMD pathogenesis (Hageman et al., 2001; Anderson et al., 2010). Immunohistochemical and proteomic studies have revealed that drusen contain numerous protein and lipid constituents that are likely to be derived via RPE biosynthesis and also by accretion of plasma components.

We recently developed a cell culture model that mimics several aspects of drusen biogenesis including the formation of sub-RPE deposits containing known drusen constituents, and deposit-mediated complement system activation (Johnson et al., 2011). The sub-RPE deposits are rich in Apolipoprotein E (ApoE), a lipid transport protein which is a ubiquitous component of human ocular drusen (Anderson et al., 2001). Exposure of the RPE cells to human serum triggers formation of C5b-9 immunoreactive terminal complement complexes that are associated with the ApoE deposits (Johnson et al., 2011). Compounds with the ability to inhibit complement activation are potential therapeutics for AMD. Therefore, we employed this model system to test the effects of compstatin family peptides on sub-RPE deposit mediated complement activation.

Compstatin family peptides are complement system inhibitors with sequence modifications that have been optimized over several years to improve anti-complement potency [reviewed in (Morikis and Lambris, 2005; Ricklin and Lambris, 2007, 2008; Qu et al., 2009)]. One compstatin peptide has been evaluated in clinical trials as a therapeutic for AMD (clinicaltrials.gov, Identifier numbers: NCT00473928 and NCT01157065) (Ricklin and Lambris, 2007, 2008; Chi et al., 2010; Zarbin and Rosenfeld, 2010; Yehoshua et al., 2011; Qu et al., 2013). Compstatin inhibits the activation of the complement system, by binding to C3, the converging protein of all three complement activation pathways, and inhibiting the cleavage of C3 to C3a and C3b by C3 convertase complexes. The mechanism of inhibition may be steric, by directly blocking convertase access to C3 or by blocking access of the convertase catalytic site to the C3 scissile bond, and may involve conformational changes (Janssen et al., 2007; Ricklin and Lambris, 2008). The mechanism of binding between compstatin peptides and their target complement protein C3 is dominated by hydrophobic interactions, as well as hydrogen bonds (Janssen et al., 2007; Tamamis et al., 2012). Compstatin family peptides are typically 13-amino acids long, and cyclization by a disulfide bridge between the second and twelfth cysteine is necessary for activity (Sahu et al., 1996; Morikis et al., 1998; Sahu et al., 2000; Morikis et al., 2002). Seven of the 13 amino acids of compstatin family peptides have been shown to be indispensible for inhibitory activity in earlier studies (Morikis and Lambris, 2002; Morikis et al., 2002; Morikis et al., 2004; Morikis and Lambris, 2005). A major breakthrough in the development of the most potent compstatin peptides was the incorporation of aromatic amino acids, tyrosine and tryptophan, at position 4 of the sequence (Klepeis et al., 2003; Klepeis et al., 2004; Mallik et al., 2005), and subsequently methylation of the tryptophan at position 4 (Katragadda et al., 2006). Although these improvements resulted in a peptide with increased binding affinity and inhibitory activity (Magotti et al., 2009), the efficacy of this peptide is compromised by its propensity to precipitate in aqueous solutions. We attribute this self-aggregation to the incorporation of a methylated tryptophan at position 4, which, together with a second tryptophan at position 7 and a hydrophobic cluster at the linked termini (positions 1-4, 12, 13), increases the overall hydrophobic character of the peptide, and decreases its aqueous solubility.

We recently performed computational and rational design studies of compstatin peptides that showed that addition of tryptophan residues at the termini (sequence positions 1 and 13) results in potent inhibiting peptides, evidenced by surface plasmon resonance and ELISA studies (Bellows et al., 2010a; López de Victoria et al., 2011), but aggregation issues were present even in the absence of methylation at position 4. We also performed multi-trajectory molecular dynamics (MD) simulations to identify the binding properties of several of the newly designed peptides at atomic resolution and with the inclusion of conformational sampling (Tamamis et al., 2012). These studies not only revealed key structural/physicochemical and geometric elements of the peptide-C3 binding cavity, but also suggested that a di-serine N-terminal extension and arginine replacement at the N-terminus produce additional contacts that improve the stability of the complex.

Leveraging data from our recent (Bellows et al., 2010a; Tamamis et al., 2010; López de Victoria et al., 2011; Tamamis et al., 2012) and other studies of compstatin family peptides (Sahu et al., 1996; Morikis et al., 1998; Furlong et al., 2000; Sahu et al., 2000; Morikis and Lambris, 2002; Morikis et al., 2002; Klepeis et al., 2003; Soulika et al., 2003; Klepeis et al., 2004; Morikis et al., 2004; Mallik et al., 2005; Morikis et al., 2005; Morikis and Lambris, 2005; Katragadda et al., 2006; Janssen et al., 2007; Ricklin and Lambris, 2008; Magotti et al., 2009; Qu et al., 2009), including MD simulation studies based on the structure of free (Mallik et al., 2003; Mallik et al., 2005; Mallik and Morikis, 2005; Song et al., 2005; Tamamis et al., 2007) and C3c-bound compstatin (Tamamis et al., 2010; Tamamis et al., 2011; Tamamis et al., 2012), we furthered the optimization of compstatin analogs using MD simulations. Our goal in this work is to increase the polarity/hydrophobicity ratio in the peptide sequence without compromising the essential hydrophobic contacts with C3. Given the limited space for sequence optimization of the already highly optimized 13-amino acid compstatin peptides, and taking into account the new binding features of the N-terminal arginine and N-terminal dipeptide extension, we reasoned that introduction of polar amino acids at positions 1, 0, and -1 would achieve our goal to increase solubility and, therefore, reduce or eliminate aggregation.

We present herein the screening results for complement inhibition of selected promising peptides using complement ELISAs and hemolytic assays. In addition, these peptides were screened in the aforementioned human RPE cell-based assay that approximates the disease characteristics of AMD. Given that compstatin is known to exhibit species specificity, and is not active in non-primate species (Sahu et al., 2003; Tamamis et al., 2010), the RPE cell-based assay is advantageous as an initial screen for efficacy of the designed peptides in a human, ocular-like microenvironment, prior to advancing to experiments with primates and clinical testing. Additionally, we tested the peptide lipophilicities using reversed phase high performance liquid chromatography (RP-HPLC), as a measure of relative peptide hydrophobicity. Finally, we present molecular insights on the interactions between the N-terminal replacements/extensions and C3, based on the results of the MD simulations.

2. Materials and Methods

2.1 Peptide synthesis

Compstatin family peptides were custom synthesized and characterized using liquid chromatography – mass spectrometry by Abgent Inc. (San Diego, CA, USA). The parent compstatin peptide (control) was purchased either from Abgent (for C3b, C5b-9 ELISAs and hemolytic assay) or from TOCRIS Bioscience (Bristol, UK; for RPE cell-based assay). The peptides were acetylated at the N-terminus and amidated at the C-terminus, with the exception of parent compstatin control, which was not acetylated at the N-terminus. All peptides were cyclized through a disulfide bridge between Cys2 and Cys12. Peptides containing methylated tryptophan (methylated-Trp) were synthesized using Fmoc-1-methyl-

DL-tryptophan, and the resulting mixture of peptides containing D-methylated-Trp and L-methylated-Trp were subsequently purified to obtain peptides containing only the L-enantiomer. Additional characterization of the peptides was performed using HPLC and NMR (see below). The peptide sequences are shown in Table 1. Note, that the Roman numeral naming scheme of the peptides is different from that of our previous publication (López de Victoria et al., 2011).

2.2 C3b and C5b-9 ELISAs

Inhibition of the complement alternative pathway (AP) by compstatin family peptides was assayed by ELISA. Peptides were dissolved in phosphate buffered saline (PBS, 150 mM). Initial peptide concentrations were calculated using the Beer–Lambert Law with an extinction coefficient of 5,500 (1 / M·cm) for Trp and 5,470 (1 / M·cm) for methylated-Trp (Marmorstein et al., 1987) present in the sequence, at 280 nm. Nunc Maxisorp 96-well plates were coated with 1 μg lipopolysaccharides (LPS) from *Salmonella enteriditis* for ~16 h at room temperature. Plates were washed three times with PBS/0.05% Tween-20 (PBS-T) between each step. Plates were blocked with 4% bovine serum albumin (BSA) in PBS-T for 1 h at 37°C. Serial peptide dilutions were performed in 96-well plates, using gelatin veronal-buffered saline with 5 mM $MgCl_2$ and 10 mM EGTA (GVBS-MgEGTA). Normal human serum (Complement Technology Inc., Tyler, TX, USA) was diluted in GVBS-MgEGTA and mixed with compstatin serial dilutions to a final concentration of 30%. Serum diluted in GVBS-MgEGTA and GVBS (containing 20 mM EDTA) were used as positive and negative controls for complement activation, respectively. Dilutions were preincubated for 15 minutes at room temperature, transferred to ELISA plates, and incubated for 1 h at 37°C. Generation of C3b and C5b-9 were assayed using horseradish peroxidase (HRP)-conjugated anti-C3 (MP Biomedicals, Solon, OH, USA) and anti-C5b-9 aE11 (Abcam, Cambridge, MA, USA), respectively. Plates were washed and incubated with either anti-C3-HRP (1:5000 in 1% BSA/PBS-T) or anti-C5b-9 (1:1000 in 1% BSA/PBS-T) for 1 h at 37°C. For C5b-9 detection, primary antibody incubation was followed by incubation with anti-mouse-HRP (BioRad, Hercules, CA, USA) for 1 h at 37°C (1:5000 in 1% BSA/PBS-T). Bound C3b and C5b-9 were quantified using a 3,3',5,5'-tetramethylbenzidine substrate solution containing urea hydrogen peroxide in 0.11 M sodium acetate buffer, followed by a 1 N H_2SO_4 acid stop. Plates were measured spectrophotometrically at 450 nm. Percent inhibition of C3b and C5b-9 deposition was plotted against peptide concentration and the data was fitted to a logistic dose response curve with Prism software (GraphPad, San Diego, CA, USA) to determine IC_{50} values.

2.3 Hemolytic Assays

Inhibition of complement was also measured via lysis of erythrocytes. Rabbit erythrocytes (Complement Technology Inc., Tyler, TX, USA) were washed in PBS and resuspended in veronal-buffered saline with 5 mM $MgCl_2$ and 10 mM EGTA (VBS-MgEGTA). Peptide and serum dilutions were prepared as described above, and 1×10^7 erythrocytes were added to each serum/peptide mixture. Erythrocytes diluted in sterile deionized water and in VBS-MgEGTA were used as positive and negative controls for lysis, respectively. Plates were incubated for 20 minutes at 37°C, and centrifuged at 2500×g for 10 minutes. Supernatants were diluted 1:2 and absorbance was measured at 405 nm.

2.4 RPE cell culture

The *in vitro* drusen biogenesis model was employed as previously described (Johnson et al., 2011). Human fetal RPE cells (Advanced Bioscience Resources, Alameda, CA) were cultured on Millipore HA porous supports (Millipore, Cat # PIHA 01250) in Miller medium (Maminishkis et al., 2006) supplemented with 5% fetal calf serum (FCS). Cultures derived from three different donor eyes were employed. Cells were rinsed with warm, sterile PBS

and the insert membrane was excised with a scalpel and cut into small (~ 4 mm^2) pieces which were placed in wells of a 96-well plate. To minimize effects of inter-culture variability, samples prepared from a single membrane were utilized for each experiment. The samples were rinsed in PBS and then exposed individually to the library of compstatin family peptides at 1 μM in FCS-free Miller medium containing 10% human complement serum (Innovative Research, Cat # IPLA-CSER AB, Lot # L12402). In preliminary experiments, compstatin family Peptides I, III, VI, VII, VIII, IX, and Parent (Table 1), were tested in the RPE cell assay at 100 μM and titrated by C5b-9 ELISA over a concentration range of 0.04-130 μM (data not shown). The 1 μM concentration employed was selected based on these results, showing it to be in the linear range of inhibitory concentrations. Also from this assessment, we selected as most promising Peptide VI, as well as Peptides I and III, for further studies. Peptides I and III were chosen for comparative studies to Peptide VI, because they contain an arginine residue at position 1. Our goal was to determine whether peptides containing arginine at position -1 (Peptide VI) or at position 1 (Peptides I and III) were potent complement inhibitors using the RPE cell assay and had improved aqueous solubility compared to previously known potent analogs. Negative control cells were exposed to Miller medium + 5% FCS; positive control cells were exposed to Miller medium + 10% human complement serum without inhibitory peptides. Experimental and control medium/inhibitor solutions were pre-mixed on a rocker at room temperature for 30 min, then warmed to 37°C, prior to placement on the samples and incubation for ~ 24 hrs at 37°C in a 7.0% CO_2 incubator. Following the incubation period, the medium was removed and stored frozen prior to ELISA analysis. The cell/membrane samples were rinsed in PBS, fixed in cold 4% paraformaldehyde (PFA) in PBS for 20 min, and stored in 0.4% PFA until use in immunohistochemical assays.

2.5 Immunohistochemistry

Fixed samples were rinsed several times in PBS, embedded in 10% agarose (Type XI, Sigma-Aldrich, Cat # A3038) and sectioned at 100 μm on a vibratome. Sections were blocked with normal donkey serum (1/20 in PBT: PBS containing 0.5% bovine serum albumin and 0.1% Triton X-100) overnight at 4°C. The sections were then co-incubated in two primary antibodies (polyclonal goat anti-ApoE, Millipore Cat # AB947; 1/1000 in PBT, and mouse monoclonal anti-C5b-9 aE11, Dako Cat # MO777; 1/200 in PBT) overnight at 4°C, then rinsed in PBT and co-incubated in secondary antibodies (Alexa Fluor 546-conjugated donkey anti-goat IgG and Alexa Fluor 488-conjugated donkey anti-mouse IgG, both 1/200 in PBT; Life Technologies Cat # A-11056 and # A-21202) overnight at 4°C. Sections were rinsed in PBT, stained with Hoechst 33342 (Life Technologies Cat # H3570), and mounted on slides with Prolong Gold (Life Technologies Cat # P36930).

2.6 Confocal imaging and analysis

Samples were imaged on an Olympus FV1000 confocal laser scanning microscope. A total of 154 single-plane images were acquired at a resolution of 1024×768 pixels and the digital image files were saved in 24-bit tiff format. Digital image analysis was performed with MetaMorph software (Molecular Devices, Sunnyvale, CA). For the analysis, a standard measurement region, which included both the RPE cell monolayer and all of the adjacent sub-cellular deposits, was applied to each image. The Set Threshold Color Tool was utilized to analyze each color channel separately; the threshold tool creates a boundary around the objects being measured (i.e. sub-cellular deposits) on the basis of color intensity. The upper threshold was set so that the entire deposit area was selected; then the lower threshold was set to exclude background fluorescence. These settings allowed the isolation of deposit-associated fluorescence and independent measurement of the area and intensity of C5b9 immunofluorescence in the green channel and ApoE immunofluorescence in the red channel (see Table S1). The ApoE threshold was standardized using the negative control samples.

The positive control samples, which contained the highest levels of C5b-9 immunoreactivity, were used to standardize the C5b-9 threshold. Positive and negative control standards and the associated thresholds were independently established for each cell line for each experiment. The sum of the pixel intensities within the threshold limits (integrated area) was used in statistical analyses. For each image, the integrated area of C5b-9 was normalized to the ApoE area and the ratio of C5b-9/ApoE intensity was expressed as a percentage of the positive control sample. Statistical analysis of the data from each of the treatment groups was performed using a one-way ANOVA calculated using Tukey's test for multiple comparisons. A p value <0.05 was considered to be of statistical significance. To assess variability in the amounts of sub-cellular deposits, the ApoE fluorescence data was analyzed and area values for the seven treatment groups were compared. This analysis demonstrated that there was not a statistically significant difference in the ApoE deposit load among the seven treatment groups examined [$F(6,14) = 0.363$, p=0.89] (Figure S1).

2.7 Soluble C5b-9 ELISA of the RPE cell-based assay medium

Experimental medium solutions were diluted 1/625 in assay diluent and quadruplicate ELISAs were performed using an OptEIA C5b-9 ELISA kit (BD Biosciences, Cat # 558315). Plates were read at 450 nm, with absorbance at 570 nm subtracted for wavelength correction, on a BioRad Benchmark plate reader. C5b-9 concentrations were calculated using a standard curve generated using purified human C5b-9. Data was expressed as a percentage relative to the positive (human serum only) control. Means and standard errors for data from the three RPE donor cells were calculated and graphed using SigmaPlot 11.0 (Systat Software, San Jose, CA), and one-way ANOVA was calculated using Tukey's test for multiple comparisons.

2.8 RP-HPLC study

The effect of the hydrophobic content of compstatin family peptides on relative lipophilicity was evaluated using RP-HPLC, a widely applied indirect technique for the determination of the lipophilicity of drugs and drug candidates (Valkó, 2004; Henchoz et al., 2009). The determination of log$P$ by RP-HPLC is based on the measurement of the retention factor k between the mobile and stationary phase (Eq. 1) of the investigated compound (Berthod and Carda-Broch, 2004)

$$\log k = \log \frac{t_R - t_0}{t_0} \quad (1)$$

where t_R is the retention time of the analyte, and t_0 is the elution time of an unretained analyte. The logarithm of the retention factor is linearly correlated with the logarithm of the partition coefficient

$$\log P - a \log k + b \quad (2)$$

where a and b are the slope and intercept of the linear equation.

The determination of log$P$ values requires calibration using structurally related compounds, and is beyond the scope of this study. Instead the log$k$ values were used to indicate the relative lipophilicities of this compstatin peptide family.

HPLC experiments were carried out using an Agilent 1100 HPLC with UV detection at 280 nm at 25 °C. Separations were performed on a Waters (Milford, MA) 4.6x150 mm XTerra MS C18 column with 5 μm pore size using a mobile phase of A: 10 mM phosphate buffer pH=7.4 containing 1% TFA, and B: acetonitrile. The purity of the peptides was verified by

an isocratic separation at 28% B and a flow rate of 1 mL/min. Solutions containing 0.6–0.8 mg/mL of Peptides I, III, VI, IX and the parent peptide were prepared in methanol and diluted 5-times with the eluent. All five peptides eluted as single peaks indicating a high degree of purity (Fig. S2).

For the determination of the relative lipophilicities a solution containing each of the peptides was prepared from the stock solutions and injected in triplicate. Isocratic elution at 24% B and a flow rate of 1 mL/min resulted in separation of the Peptides I, III, VI, IX and Parent (Fig. S3). A 0.5 mg/mL solution of aspartic acid was used as the unretained analyte for the determination of the column dead time, 1.439 ± 0.003 min.

Sodium phosphate monobasic, aspartic acid, methanol and acetonitrile were obtained from Fisher Scientific (Pittsburgh, PA). Trifluoroacetic acid (TFA) was purchased from Acros (Geel, Belgium). HPLC-grade Burdick and Jackson water was used for the HPLC analysis (Morristown, NJ).

2.9 NMR study

NMR spectroscopy was used to confirm peptide purity. Although the HPLC separations suggested that the peptides were of high purity as a single chromatographic peak was observed for each sample, the possibility of coelution of the desired peptide and structurally related impurities cannot be discounted. Because of the sensitivity of chemical shifts to subtle structural changes, ^{1}H NMR spectroscopy provides an excellent measure of peptide purity. ^{1}H NMR spectra were acquired for separate solutions of each peptide prepared by dissolving 1 mg samples into 600 μL 50 mM phosphate buffer containing 10% D_2O and 0.4 mM 2,2-dimethyl-2-silapentane-5-sulfonate-d_6 sodium salt (DSS) as a reference compound. The pH of the phosphate buffer was set to 6.5 using NaOD. ^{1}H NMR spectra were recorded at 22 °C with a Bruker Avance spectrometer operating at ^{1}H frequency of 600.01 MHz using a triple resonance inverse probe. Excitation sculpting was used for water suppression (Bruker pulse program *zgesgp*) (Hwang and Shaka, 1995). Spectra were collected into 32,768 points using 64 scans with a spectral window of 12 ppm, were processed in 65,536 points and multiplied with an exponential function equivalent to 0.5 Hz line broadening.

Deuterium oxide and NaOD were obtained from Cambridge Isotope Laboratories (Andover, MA), DSS was purchased from Sigma Chemical Company (St. Louis, MO). Water was HPLC grade from Burdick & Jackson (Honeywell, Morristown, NJ).

The samples used to measure C3b and C5b-9 ELISAs and hemolytic lysis assays presented here (Peptides I, III, VI, IX, and Parent) were tested with HPLC and NMR, as discussed above and were found to be pure (Figs. S2-S4). The samples used for the RPE cell assays were from an older preparation and some appeared to have an impurity in HPLC experiments, which was not due to aggregates. We have estimated the impurity populations of the old Peptides III and VI was 15% and 33% using the HPLC chromatograms. Nevertheless, the relative potencies of the peptides were similar in C3b ELISA experiments using the two sample preparations.

2.10 Molecular dynamics simulations

Molecular dynamics simulations were performed for Peptides III and VI, using explicit water solvation as described elsewhere (Tamamis et al., 2010; Tamamis et al., 2011; Tamamis et al., 2012). The molecular mechanics program CHARMM c35b5 (Brooks et al., 2009) was used for the simulations, with the CHARMM22 all-atom force field (MacKerell et al., 1998), including a CMAP backbone ϕ/ψ energy correction (Mackerell et al., 2003) and indole parameters (Macias and MacKerell, 2005). Match server was used to derive the topology and parameters for the methylated tryptophan aromatic ring (Yesselman et al.,

2012). The simulation protocol and force field specifications were as described in (Tamamis et al., 2010; Tamamis et al., 2011; Tamamis et al., 2012). As in (Tamamis et al., 2012), loop C3 369-378 was unrestrained during the simulations since it is in proximity to the N-terminus of the peptides. For Peptide III, five 7-ns trajectories, starting from the same initial conformation with different equilibration times, were generated to a total of 35 ns simulation time. For Peptide VI, five 10-ns trajectories, starting from the same initial conformation with different equilibration times, were generated to a total of 50 ns simulation time. A total of 700 and 1,000 snapshots were analyzed for III and VI, respectively, extracted every 50 ps per trajectory. Percent occupancies were calculated for hydrogen bonds, as well as averaged intermolecular interaction energies, using homemade scripts. Molecular visualization was performed using the program VMD (Humphrey et al., 1996).

2.10.1 Initial coordinates—For Peptide III, the protein and ligand atoms (with the exception of Arg1 side chain), were initially placed according to the crystallographic structure of the Ac-V4W/H9A Compstatin: human C3 complex (PDB code 2QKI) (Janssen et al., 2007). The Arg1 side chain was placed with the aid of program SCWRL 4.0 (Krivov et al., 2009). For Peptide VI, the protein and ligand atoms (with the exception of the Arg-1 side chain) were initially placed at a structure taken from the simulation of the Ac-SS-ICVWQDWGAHRCT-NH_2: human C3 complex (Tamamis et al., 2012); that simulation itself was based on the crystallographic structure of the Ac-V4W/H9A Compstatin: human C3 complex (PDB code 2QKI) (Janssen et al., 2007). The employed structure had the lowest association free energy, as determined in the Molecular Mechanics-Generalized Born/Surface Area (MM-GBSA) approximation [see Eq. (4,5) of (Tamamis et al., 2012)]. The Arg-1 side chain was placed with the aid of program SCWRL 4.0 (Krivov et al., 2009).

2.10.2 Computation of interaction free energies of protein and ligand residue pairs—The interaction free energies between two (*R* and *R'*) residues are computed in the MM-GB/SA approximation, as described (Kieslich et al., 2012; Tamamis et al., 2012) using the equation

$$\Delta G_{RR'}^{\text{inte}} = \underbrace{\sum_{i\in R}\sum_{j\in R'}\left(E_{ij}^{Coul}+E_{ij}^{GB}\right)}_{\Delta G_{RR'}^{polar}} + \underbrace{\sum_{i\in R}\sum_{j\in R'}E_{ij}^{vW}+\sigma\sum_{i\in R,R'}\Delta S_i}_{\Delta G_{RR'}^{nonpolar}} \quad (3)$$

The first and second group of terms on the right-hand side of Eq. (3) describe, respectively, polar and nonpolar interactions between *R* and *R'*, where Coul denotes Coulombic, GB denotes generalized Born, S is the solvent accessible surface area, and σ is a surface tension coefficient. In our calculations, *R* corresponded to a ligand residue and *R'* corresponded to a protein residue. To compute the GB term (Im et al., 2003) term in Eq. (3), we included all protein and ligand atoms and set the charge to zero for atoms other than those belonging to residues *RR'*, *R* and *R'*, respectively, in each calculation of the terms on the right-hand side terms of Eq. (3). The last term contains the difference in solvent accessible surface areas of groups *R* and *R'* in the complex and unbound states. Free-energy values were averaged over all trajectories. We decomposed the total interaction free energies into polar and nonpolar interaction free energy components and the results are presented in two-dimensional maps.

3. Results

3.1 Peptide design

The design of the new compstatin peptides was inspired by our recent studies that include (i) the application of two-stage computational frameworks for protein design that are based on

sequence selection, fold specificity, and approximate binding affinity calculations (Bellows et al., 2010a); (ii) rational design based on structural/physicochemical analysis – activity relations (López de Victoria et al., 2011); and (iii) structural and binding analysis using molecular dynamics simulations (Tamamis et al., 2012). These studies identified new active compstatin family peptides with novel features, such as introduction of tryptophans at positions 1 and 13, arginine at position 1, and an N-terminal di-serine extension. Some of these analogs suffer from solubility/aggregation problems, owing to increased hydrophobicity content conferred by the presence of up to four tryptophans. Nevertheless, these studies revealed three new sites of optimization in the compstatin peptide sequence at positions 1, 0, and −1. We reasoned that incorporation of polar amino acids at positions 1, 0, and −1, while maintaining the amino acids that are involved in hydrophobic contacts with C3, would aid in balancing the polarity/hydrophobicity ratio and in improving solubility. The choice of amino acids for positions 1, 0, and −1 was based on our previous molecular dynamics simulations (Tamamis et al., 2012) and supported by new molecular dynamics simulations, such as those described below, for Peptides III and VI. Methodological details are given elsewhere for the two-stage computational frameworks (Bellows et al., 2010a; Bellows et al., 2010b; Bellows-Peterson et al., 2012), biochemical assays (López de Victoria et al., 2011), and MD simulations (Tamamis et al., 2010; Tamamis et al., 2011; Tamamis et al., 2012).

Table 1 shows the sequences of the peptides studied. With the exception of Parent, the sequences of Table 1 contain either Trp or methylated-Trp at position 4 and Ala at position 9. The new sequences include N-terminal replacements of Ile with Arg (Peptides I and III), as well as N-terminal extensions (Peptides IV, VI-VIII). The latter include the Ser-Ser (Peptide IV and VIII) and Arg-Ser (Peptides VI and VII) extensions. Two of the Arg-Ser extension sequences also incorporate N-terminal replacements of Ile with Arg (Peptides VII and VIII). These sequences are modeled after the sequence of the most potent peptides comprised entirely of natural amino acids [control Peptide IX; (Mallik et al., 2005)] and the most potent peptide to-date, which is similar to Peptide IX but with methylated-Trp at position 4, with methylation being attached at the indole nitrogen (Katragadda et al., 2006). Four of the new sequences in Table 1 incorporate methylated-Trp at position 4 (Peptides III, VI-VIII), in an effort to maintain high potency, and six contain polar amino acids at positions −1, 0, and 1 (Peptides I, III, IV, VI-VIII). We also tested two more sequences that contain hydrophobic amino acids (Trp or methylated-Trp) at the N-terminus or N-terminal extension for contrasting comparisons (Peptides II and V), which showed reduced solubilities. The incorporation of tryptophans at the amino terminus was suggested by our recent previous work (Bellows et al., 2010a; López de Victoria et al., 2011; Tamamis et al., 2012).

In preliminary C3b ELISA experiments, Peptides I-IX demonstrated comparable potencies, within up to 3-fold IC_{50} differences. We selected for preliminary RPE cell culture experiments Peptides I, III, VI, VII, and VIII, which contained Arg at the N-terminus or N-terminal extension, together with control Peptide IX and Parent. The remaining peptides were discarded because of solubility issues (Peptides II and V) or because they did not contain Arg at the N-terminus or N-terminal extension (Peptides II and IV). Based on the preliminary RPE cell assay studies (see Materials and Methods) a reduced number of peptides (Peptides I, III, and VI) was selected, for more quantitative C3b and C5b-9 ELISA, hemolytic assay, and RPE cell-based assay studies, together with control Peptide IX and Parent for comparison. These studies are described in detail below.

3.2 Analysis of complement inhibition by C3b and C5b-9 ELISA, and erythrocyte lysis assay

Since compstatin family peptides are known to selectively inhibit the complement alternative pathway (AP), we performed ELISAs and erythrocyte lysis assays to examine AP inhibition. In all assays, MgEGTA was used to chelate Ca^{2+} ions required for classical/lectin pathway complement activation, while providing Mg^{2+} necessary for AP activation. ELISAs allow for direct detection of C3b and C5b-9 formed during AP activation, while erythrocyte lysis assays provide a functional assessment of AP-mediated hemolysis in serum. Figure 1 shows the C3b and C5b-9 ELISA and erythrocyte lysis data for Peptides I, III, VI, IX, and Parent. Table 2 summarizes the IC_{50} values derived from the three different assays. Parent exhibited significantly less complement inhibition than all other peptides in all three assays. Newly-designed peptides (Peptides I, III, and VI) showed similar IC_{50} values to Peptide IX, with Peptide I having a slightly higher IC_{50} than the others in all cases. The relative potencies of the peptides, based on the measured IC_{50} values, are consistent across all three assays (Peptide III ~ Peptide VI ~ Peptide IX > Peptide I > Parent). Based on the assay conditions used in this study, peptides inhibited C5b-9 formation with moderately better efficacy than formation of C3b, while slightly higher concentrations were necessary to inhibit AP-mediated hemolysis. It is also noteworthy that while C3b and C5b-9 inhibition by Parent was about 10- to 15-fold less than other peptides in ELISA, only a 4- to 6-fold difference was observed for hemolysis.

3.3 Complement inhibition in the RPE cell model

Exposure of RPE cell cultures to human serum leads to complement activation, as evidenced by the formation of subcellular deposit-associated C5b-9 (Johnson et al., 2011). Deposit-associated C5b-9 immunofluorescence was quantified using confocal microscopy and normalized to the fluorescence signal for ApoE (a ubiquitous deposit marker). In the presence of active compstatin family peptides, the amount of deposit-associated C5b-9 is reduced, proportionally to the peptide potencies. Figure 2 shows examples of confocal immunofluorescence images of sub-RPE deposit-associated C5b-9.

Table 3 and Fig. 3 show the results of the RPE cell experiments for the aforementioned peptides. Peptides III, VI, and IX showed significantly more complement inhibition than Parent, reducing the C5b-9 deposits to approximately 15–20% of the positive control (human serum without inhibitory peptides). The effect of methylated-Trp4 in complement inhibition is evident when comparing the confocal imaging data of Peptides III and VI against those of Peptide I, which contains unmethylated Trp (Table 1). The confocal microscopy data reveal a large range of inhibition at the level of the sub-RPE deposits, and markedly discriminate the potencies of the peptides.

The one-way ANOVA revealed a significant effect of the complement inhibitory peptides on deposit-associated C5b-9 formation [$F(5,12) = 26.4$, $p < 0.001$]. In the presence of Parent, deposit-associated complement activation was reduced to 83% of the positive control (mean ± S.E.M. = 83.2 ± 5.9), but this difference was not statistically significant. However, Peptides I (55.3 ± 12.3), III (20.0 ± 6.8), VI (14.9 ± 5.6), and IX (21.1 ± 6.3), all exhibited significantly more inhibition, and all were statistically different from Parent ($p < 0.001$). Peptides III, VI, and IX exhibited the greatest potencies and were not significantly different from each other.

Overall, the relative potencies derived from the RPE cell-based assay, C3b and C5b-9 ELISAs, and hemolytic assay experiments are in agreement and they follow the order Peptide III ~ Peptide VI ~ Peptide IX > Peptide I > Parent.

3.4 Analysis of complement inhibition by soluble C5b-9 ELISA of the RPE cell-based assay medium

We also performed C5b-9 ELISAs of the RPE cell assay medium (Table 3, Fig. 4). A narrow range of inhibition was observed in these C5b-9 data, compared to the confocal microscopy data, likely reflecting background turnover of complement in the liquid phase as opposed to that directly associated with the sub-RPE deposits. Nevertheless, the one-way ANOVA showed a significant effect of the inhibitory peptides on soluble C5b-9 formation [$F(5,12) = 144.2$, $p < 0.001$]. This parallel analysis of soluble C5b-9 in the experimental medium solutions also showed the level of inhibition by Parent to be less than that of the experimental peptides. In the presence of Parent, C5b-9 levels were reduced to 89% of the positive control (mean ± S.E.M. = 88.5 ± 0.76, $p = 0.011$). All of the experimental peptides were more inhibitory, I (61.4 ± 2.3), III (50.0 ± 0.8), VI (44.6 ± 3.2), IX (51.9 ± 2.2) and all were statistically different from Parent ($p < 0.001$).

3.5 Lipophilicity measurements using RP-HPLC

We used RP-HPLC to measure the hydrophobicity/lipophilicity content of the compstatin family peptides. The retention of a compound in RP-HPLC depends on its hydrophobicity/lipophilicity content, and is correlated to the octanol–water partition ratio (Berthod and Carda-Broch, 2004; Valkó, 2004; Henchoz et al., 2009). Lipophilicity describes the partitioning of a compound between an aqueous and a lipidic/hydrophobic environment, and is an essential physicochemical parameter to determine pharmacokinetic behavior according to ADME (absorption, distribution, metabolism, excretion) characterization. Because the compstatin family peptides consist of a hydrophobic and a polar surface (Morikis and Lambris, 2002; Morikis et al., 2002; Morikis et al., 2004), their ability to bind to the hydrophobic cavity of C3, while maintaining a solvent-exposed face has been evaluated here as lipohilicity content, measured by RP-HPLC. In addition, lipohilicity is inversely proportional to aqueous solubility, and therefore can be used to estimate solubility of the peptides in their free (unbound) state.

Table 4 shows the retention times (t_R) and retention factors (k) for Peptides I, III, VI, IX, and Parent. These, and data for the whole set of peptides of Table 1 (not shown), suggest that the major factors governing hydrophobicity of the peptides are the number of tryptophan and methylated-tryptophan residues in the sequence, which increases hydrophobicity, and the net charge of the peptide, which decreases hydrophobicity. Peptides containing two or more tryptophans are the most lipophilic, and introduction of arginines in the sequence results in decreasing lipohilicity. Parent is the least lipophilic (Table 4).

The relative lipophilicities of Peptides I, III, VI, IX, and Parent are inversely consistent with solubilities as determined via concentration measurement (absorbance at 280 nm) of saturated peptide solutions, with Peptides I, III, and Parent having approximate aqueous solubilities of > 1 mM, Peptide VI > 500 μM, and Peptide IX < 500 μM.

3.6 Molecular dynamics simulations

Recent MD studies have provided insights into the role of arginine at position 1 (Peptide I, Table 1) and the diserine extension at positions 0 and −1 (Peptide IV, Table 1) (Tamamis et al., 2012). The MD studies have shown that an Arg1 substitution (Peptide I) maintains the interactions with C3 observed in control Peptide IX, with a new salt bridge being observed between Arg1 and C3 Asp349 (Tamamis et al., 2012). As the presence of a methyl group at Trp4 has been reported to enhance binding affinity compared to control Peptide IX (Katragadda et al., 2006), we performed MD simulations of C3-bound Peptide III, which has a methyl group at Trp4 compared to Peptide I. Similarly, Peptide IV also maintains the interactions with C3 observed in control Peptide IX, with a new hydrogen bond being

observed between Ser0 and C3 Asn390 (Tamamis et al., 2012). These additional interactions involving N-terminal residues, contribute to increased computed binding affinity with regard to Peptide IX-C3 complex. Critical analysis of the contacts of the diserine extension with C3 residues led us to replace serine by arginine at position −1, and additionally investigate Peptide VI in complex with C3 using MD simulations. Besides increased intermolecular contacts and computed binding affinities, the introduction of the polar-charged arginine residues at positions 1 (Peptide III) or −1 (Peptide VI) also contribute to increased peptide solubilities, a desired property of the new designs.

We performed MD simulations to understand the molecular interactions of the two most promising new peptides (Peptides III and VI). Figure 5 shows representative MD structures of Peptides III, VI and control Peptide IX, depicting intermolecular hydrogen bonding patterns and nonpolar pockets within the binding site. Typically, the 13-residue compstatin peptides form intermolecular contacts with four C3 sectors (Tamamis et al., 2010; Tamamis et al., 2012), as is the case for control Peptide IX (Fig. 5E, F). For Peptide III, the incorporation of a methyl group at Trp4, in conjunction with an Ile1Arg substitution, leads to additional intramolecular interactions between peptide residues and additional intermolecular peptide-C3 interactions, compared to control Peptide IX. The methyl group of Trp4 fits between the disulfide bridge Cys2-Cys12 of the ligand and residues His392 and Pro393 of C3. Owing to the favorable Cys2- methylated-Trp4 interaction, the N-terminus of the ligand is displaced (Fig. 5A, B, towards segments colored in blue, orange, and green on the right-hand side of each panel) with regard to Peptide IX (Fig. 5 C, D); the root mean square displacement of atom Arg1 Cα is 2.3 Å. Therefore, the side chain of Arg1 of Peptide III is favored to form a new highly interacting salt bridge with Glu372 of the fifth C3 sector (Fig. 5A; Table 5). This finding is in contrast to the Arg1-Asp349 salt bridge, which is present in the absence of methyl group at Trp4 (Peptide I) (Tamamis et al., 2012). For Peptide VI, the two-residue Arg-Ser N-terminal extension forms additional contacts with a fifth C3 sector (Fig. 5C, D; Table 5). These contacts include a strong salt bridge between the side chains of Arg-1 and C3 residue Glu372 of the fifth sector, and contribute to increased stability of the complex compared to control Peptide IX (Tamamis et al., 2010). Figure 6 shows the interaction free energy maps of intermolecular interactions between protein residues and ligand residues. Panels 6A, B present the polar and Panels 6C, D present the nonpolar interaction free energies of Peptides III and VI, respectively. The strongest pairwise intermolecular interactions, are formed between the newly introduced Arg1/Arg-1 residues of Peptides III and IV, respectively, and C3 Glu372 (Fig. 6). Similarly to Peptide III, the Trp4 methyl group of Peptide VI fits between the disulfide bridge residues Cys2-Cys12 of the ligand and residues His392 and Pro393 of C3. It is worth noting that Ile1 of Peptide VI is not destabilized from its initial position as it is attracted to C3 residues Pro347 and Asn390 on the one side, and C3 residues Leu454, Leu492, as well as compstatin residue His10, on the other side.

4. Discussion

This study was motivated by the impetus to design and identify new compstatin analogs with improved binding, complement inhibition, and solubility characteristics. The scope of the design was two-fold; first, to promote binding to the target protein C3 through key amino acid side chain interactions, and second, to enhance solubility compared to previously known compstatin analogs, by improving the peptide polarity/hydrophobicity ratio. Our design is based on the application of two-stage computational frameworks (Bellows et al., 2010a), use of biochemical binding and inhibitory assays (López de Victoria et al., 2011), and MD simulations of peptide- C3 complexes (Tamamis et al., 2012), which have demonstrated that either an arginine substitution at position 1 or a diserine extension at the N-terminus lead to novel binding contacts with C3. In the present study, the introduction of

an arginine either at position 1 or at position –1 of N-terminal dipeptide extensions, in conjunction with a presence of methyl group at the side chain of Trp4, both promote the formation of salt bridges with Glu372, located on C3.

A total of ten peptides were studied, three of which are N-terminal replacements (Peptides I-III), five are N-terminal extensions (Peptides IV-VIII), and two are positive controls (Peptide IX and Parent; Table 1). One peptide from the N-terminal replacements and one from the N-terminal extensions were introduced in a previous study (Peptide I and Peptide IV, respectively; (Tamamis et al., 2012)). From the eight newly designed peptides, four have tryptophan at position 4 (Peptides I, II, IV, and V) and four have methylated-tryptophan at position 4 (Peptides III, and VI-VIII). The design of six out of eight new analogs was aimed at increasing polarity at the N-terminal sequence segment (Peptides I, III, IV, and VI-VIII), whereas the remaining two analogs were designed with an aim of increasing hydrophobicity and were used for comparison (Peptides II and V). We used two compstatin peptides as controls; Parent represents the unmodified sequence of compstatin, with non-acetylated N-terminus, valine at position 4 and histidine at position 9 (Sahu et al., 2000). The Parent control is the only non-acetylated peptide in this study (Table 1). Control Peptide IX (Mallik et al., 2005) represents the most active known compstatin analog consisting only of natural amino acids prior to this study. Its sequence is similar to Parent, but it is acetylated at the N-terminus and has tryptophan and alanine replacements at positions 4 and 9, respectively. Taking into account that the most potent compstatin analog reported to date contains a methylated-tryptophan at position 4 (Katragadda et al., 2006), we decided to incorporate methylated-Trp4 in half of the eight new peptides presented here (Table 1).

The rationale for introducing novel features in the sequence of compstatin family peptides is based on the need for improving solubility and eliminating aggregation in aqueous solutions. The previously reported most potent peptide to date, similar to Peptide IX but with methylated-Trp4, is known to possess precipitation characteristics and exhibits intravitreal deposit formation (Chi et al., 2010; Yehoshua et al., 2011; Qu et al., 2013). Consistent with these reports, we observed that this peptide exhibited low solubility and visible precipitation, based on concentration measurements of saturated aqueous solutions of the peptide (See Materials and Methods). In addition, aggregation of this peptide prohibited its testing in RPE-based cell assays. This peptide is not the only compstatin analog with solubility problems; Peptide IX is also not highly soluble and is prone to aggregation at high concentrations. Therefore, Peptides I, III, IV, and VI-VIII were designed to contain polar amino acids at positions −1, 0, and 1. The effect of polar amino acids on the lipophilicity of these peptides was assessed using RP-HPLC experiments, and was found to be in agreement with our design rationale. Saturating concentrations measured prior to ELISA and hemolysis screening confirmed relative solubilities of newly designed and control peptides.

In addition to solubility enhancement, we sought to identify analogs exhibiting potent complement inhibition. While residues at the N-terminus (and in N-terminal extensions) were optimized for peptide solubilty, key amino acids contributing to binding (Janssen et al., 2007; Tamamis et al., 2012) are maintained in the peptide sequences. Hydrophobicity was shown to be important for compstatin peptide binding to C3 in early studies based on the structure of free parent compstatin (Morikis et al., 1998; Sahu et al., 2000; Morikis and Lambris, 2002; Morikis et al., 2002; Klepeis et al., 2003; Soulika et al., 2003; Klepeis et al., 2004; Morikis et al., 2004; Mallik et al., 2005; Mallik and Morikis, 2005; Morikis and Lambris, 2005), and more recent studies based on the structure of a C3c-bound compstatin analog (Janssen et al., 2007; Ricklin and Lambris, 2008; Magotti et al., 2009; Qu et al., 2009; Bellows et al., 2010a; Tamamis et al., 2010; López de Victoria et al., 2011; Tamamis et al., 2012; Qu et al., 2013). However, as increased hydrophobic amino acid content resulted in higher potency, it also brought undesirable solubility problems.

Based on critical analysis of the structural data from the MD trajectories and the results of initial C3b ELISA studies, we selected Peptides I, III, and VI, for further evaluation of their inhibitory activities using C3b and C5b-9 ELISA and functional hemolytic assays. Peptide IX and Parent were used as controls for high and low levels of complement inhibition, respectively. ELISA results showed potent inhibition by newly designed peptides, with similar C3b and C5b-9 inhibition levels as observed for positive control Peptide IX. Parent exhibited at least 10-fold less inhibition. In functional hemolytic assays, we observed a similar trend. Irrespective of the magnitudes of complement inhibition in the various assays used in this (and other) studies, the relative efficacies of Peptides I, III, VI, IX, and Parent remained consistent.

We also used a novel human RPE cell assay and C5b-9 ELISA of the cell culture medium to evaluate the efficacy of the newly designed compstatin family peptide inhibitors of the complement system. The RPE cell assay provides an experimental model for testing complement inhibition in a cell environment that mimics AMD pathogenesis, and therefore is superior to *in vitro* ELISA-based complement inhibition assays. Confocal image analysis of C5b-9 immunofluorescence from the RPE experiments provides strong evidence for the efficacy of Peptides III, VI, and IX, with all of them being equally potent within experimental error. Our data show that methylation of Trp4 in combination with incorporation of Arg1 or Arg-1 at the N-terminus (Peptides III and VI, respectively) produces up to 85% complement inhibition at the sub-RPE deposit level. Perhaps this is an adequate level of inhibition, as it is not desirable to completely abrogate the immune response benefits of complement function in the clinic. Peptide IX (positive control) showed statistically similar complement inhibition, whereas Parent was much less effective. Given the improved solubility properties of Peptides III and VI, they may be good alternatives to the currently most potent peptide (possessing methylated-Trp4), which exhibits aggregation at high concentrations in aqueous environments.

In addition to improved solubility/lipophilicity properties, Peptides III and VI introduce a novel feature in the binding mechanism to C3, through the formation of intermolecular salt bridges between arginine at positions 1 or −1 and Glu372 of C3. These salt bridges provide additional stabilization to the C3-Peptide III and C3-Peptide VI complexes, compared to other known complexes of C3 with compstatin analogs. The novelty of the salt bridge interactions arises from the fact that Glu372 lies outside the binding pocket that was previously determined experimentally and computationally (Janssen et al., 2007; Tamamis et al., 2010; Tamamis et al., 2012). Therefore, incorporation of Arg1/−1 in the sequence of compstatin analogs is an additional contributing factor to the steric hindrance of the convertase binding to C3.

5. Conclusions

Our study presents a proof-of-concept demonstration of the utility of a novel human RPE cell-based assay in quantifying complement inhibition in an AMD-like environment. Given the species specificity of compstatin for human and primate C3, but not for murine and other non-primate C3 (Sahu et al., 2003; Tamamis et al., 2010), and therefore lack of non-primate animal models, the RPE cell assay may be a viable alternative for initial screenings in advance of testing in primates in preparation for clinical trials. The study also validates our computational protocol for the design of new potent complement-inhibiting peptides of the compstatin family. We show that incorporation of polar amino acids at the N-terminus or N-terminal extension, with arginine at positions 1 or −1, improves polarity/hydrophobicity ratio and therefore improves solubility/lipophilicity properties. In addition, the MD data provide mechanistic evidence for the function of compstatin peptides at molecular level, based on intermolecular contacts and energetic analysis. In particular, the MD structural data

depict that Peptides III and VI form strong intermolecular salt bridges between arginine at positions 1 or −1 and Glu372 of C3, which is an additional contributing factor to stability of the C3-Peptide complexes and to the steric hindrance mechanism for convertase binding. We expect that our data will form the basis for further optimization of these peptides, perhaps by incorporating additional non-natural amino acids, in search of a more potent complement inhibitor for the treatment of AMD.

Supplementary Material

Refer to Web version on PubMed Central for supplementary material.

Acknowledgments

This work was funded by a grant from the Beckman Initiative for Macular Research (BIMR Grant 1112 to DM and LVJ), and by the generous benefactors of the Center for the Study of Macular Degeneration at UC Santa Barbara. CAF acknowledges support from NIH R01-GM052032. GA and PT acknowledge financial support from a University of Cyprus grant, and use of computational resources at the Biophysics clusters of the University of Cyprus and at an IBM cluster of the Cyprus Institute (financed by the Cyprus Research Promotion Foundation grant INFRASTRUCTURE/STRATEGIC/0308/31 that is co-funded by the European Regional Development fund). RDG acknowledges support from the UCR Dissertation Year Fellowship Award. DM, RDG, ALdV, and CAK thank David Lo for continuous help with the ELISA experiments.

Abbreviation List

AMD	age-related macular degeneration
C3	complement system protein 3
C3b	the b-fragment of C3
C3c	the c-fragment of C3
FB	factor B
C5b-9	the membrane attack complex consisting of complement proteins C5b, C6, C7, C8, and C9n
AP	alternative pathway of complement activation
ApoE	apolipoprotein E, ELISA enzyme-linked immunosorbent assay
RPE	retinal pigmented epithelium
RP-HPLC	reversed phase high performance liquid chromatography
PDB	Protein Data Bank
MD	molecular dynamics

References

Anderson DH, Ozaki S, Nealon M, Neitz J, Mullins RF, Hageman GS, Johnson LV. Local cellular sources of apolipoprotein E in the human retina and retinal pigmented epithelium: Implications for the process of drusen formation. American Journal of Ophthalmology. 2001; 131:767–781. [PubMed: 11384575]

Anderson DH, Radeke MJ, Gallo NB, Chapin EA, Johnson PT, Curletti CR, Hancox LS, Hu J, Ebright JN, Malek G, Hauser MA, Rickman CB, Bok D, Hageman GS, Johnson LV. The pivotal role of the complement system in aging and age-related macular degeneration: hypothesis re-visited. Prog Retin Eye Res. 2010; 29:95–112. [PubMed: 19961953]

Bellows ML, Fung HK, Taylor MS, Floudas CA, López de Victoria A, Morikis D. New compstatin variants through two de novo protein design frameworks. Biophys J. 2010a; 98:2337–2346. [PubMed: 20483343]

Bellows ML, Taylor MS, Cole PA, Shen L, Siliciano RF, Fung HK, Floudas CA. Discovery of Entry Inhibitors for HIV-1 via a New De Novo Protein Design Framework. Biophysical Journal. 2010b; 99:3445–3453. [PubMed: 21081094]

Bellows-Peterson ML, Fung HK, Floudas CA, Kieslich CA, Zhang L, Morikis D, Wareham KJ, Monk PN, Hawksworth OA, Woodruff TM. De Novo Peptide Design with C3a Receptor Agonist and Antagonist Activities: Theoretical Predictions and Experimental Validation. Journal of Medicinal Chemistry. 2012; 55:4159–4168. [PubMed: 22500977]

Berthod A, Carda-Broch S. Determination of liquid-liquid partition coefficients by separation methods. Journal of chromatography A. 2004; 1037:3–14. [PubMed: 15214657]

Brooks BR, Brooks CL III, Mackerell AD Jr, Nilsson L, Petrella RJ, Roux B, Won Y, Archontis G, Bartels C, Boresch S, Caflisch A, Caves L, Cui Q, Dinner AR, Feig M, Fischer S, Gao J, Hodoscek M, Im W, Kuczera K, Lazaridis T, Ma J, Ovchinnikov V, Paci E, Pastor RW, Post CB, Pu JZ, Schaefer M, Tidor B, Venable RM, Woodcock HL, Wu X, Yang W, York DM, Karplus M. CHARMM: the biomolecular simulation program. J Comput Chem. 2009; 30:1545–1614. [PubMed: 19444816]

CAPT. Risk factors for choroidal neovascularization and geographic atrophy in the complications of age-related macular degeneration prevention trial. Ophthalmology. 2008; 115:1474–1479. 1479, e1471–e1476. [PubMed: 18502512]

Chi ZL, Yoshida T, Lambris JD, Iwata T. Suppression of drusen formation by compstatin, a peptide inhibitor of complement C3 activation, on cynomolgus monkey with early-onset macular degeneration. Advances in experimental medicine and biology. 2010; 703:127–135. [PubMed: 20711711]

Furlong ST, Dutta AS, Coath MM, Gormley JJ, Hubbs SJ, Lloyd D, Mauger RC, Strimpler AM, Sylvester MA, Scott CW, Edwards PD. C3 activation is inhibited by analogs of compstatin but not by serine protease inhibitors or peptidyl alpha-ketoheterocycles. Immunopharmacology. 2000; 48:199–212. [PubMed: 10936517]

Hageman GS, Luthert PJ, Chong NHV, Johnson LV, Anderson DH, Mullins RF. An integrated hypothesis that considers drusen as biomarkers of immune-mediated processes at the RPE-Bruch's membrane interface in aging and age-related macular degeneration. Prog Retin Eye Res. 2001; 20:705–732. [PubMed: 11587915]

Henchoz Y, Bard B, Guillarme D, Carrupt PA, Veuthey JL, Martel S. Analytical tools for the physicochemical profiling of drug candidates to predict absorption/distribution. Analytical and bioanalytical chemistry. 2009; 394:707–729. [PubMed: 19184676]

Humphrey W, Dalke A, Schulten K. VMD: Visual molecular dynamics. Journal of Molecular Graphics. 1996; 14:33–38. [PubMed: 8744570]

Hwang TL, Shaka AJ. Water suppression that works - excitation sculping using arbitrary wave-forms and pulsed-field gradients. J. Magn. Reson. Ser. A. 1995; 112:275–279.

Im W, Lee MS, Brooks CL 3rd. Generalized born model with a simple smoothing function. J Comput Chem. 2003; 24:1691–1702. [PubMed: 12964188]

Janssen BJ, Halff EF, Lambris JD, Gros P. Structure of compstatin in complex with complement component C3c reveals a new mechanism of complement inhibition. J Biol Chem. 2007; 282:29241–29247. [PubMed: 17684013]

Johnson LV, Forest DL, Banna CD, Radeke CM, Maloney MA, Hu J, Spencer CN, Walker AM, Tsie MS, Bok D, Radeke MJ, Anderson DH. Cell culture model that mimics drusen formation and triggers complement activation associated with age-related macular degeneration. P Natl Acad Sci USA. 2011; 108:18277–18282.

Katragadda M, Magotti P, Sfyroera G, Lambris JD. Hydrophobic effect and hydrogen bonds account for the improved activity of a complement inhibitor, compstatin. J Med Chem. 2006; 49:4616–4622. [PubMed: 16854067]

Kieslich CA, Tamamis P, Gorham RDJ, López de Victoria A, Sausman N, Archontis G, Morikis D. Exploring protein-ligand and protein-protein interactions in the immune system using molecular dynamics and continuum electrostatics. Current Physical Chemistry. 2012; 2:324–343.

Klein ML, Ferris FL 3rd, Armstrong J, Hwang TS, Chew EY, Bressler SB, Chandra SR. Retinal precursors and the development of geographic atrophy in age-related macular degeneration. Ophthalmology. 2008; 115:1026–1031. [PubMed: 17981333]

Klepeis JL, Floudas CA, Morikis D, Tsokos CG, Argyropoulos E, Spruce L, Lambris JD. Integrated computational and experimental approach for lead optimization and design of compstatin variants with improved activity. J Am Chem Soc. 2003; 125:8422–8423. [PubMed: 12848533]

Klepeis JL, Floudas CA, Morikis D, Tsokos CG, Lambris JD. Design of peptide analogues with improved activity using a novel de novo protein design approach. Ind Eng Chem Res. 2004; 43:3817–3826.

Krivov GG, Shapovalov MV, Dunbrack RL Jr. Improved prediction of protein side-chain conformations with SCWRL4. Proteins. 2009; 77:778–795. [PubMed: 19603484]

López de Victoria A, Gorham RD Jr, Bellows-Peterson ML, Ling J, Lo DD, Floudas CA, Morikis D. A new generation of potent complement inhibitors of the Compstatin family. Chem Biol Drug Des. 2011; 77:431–440. [PubMed: 21352502]

Macias AT, MacKerell AD Jr. CH/pi interactions involving aromatic amino acids: refinement of the CHARMM tryptophan force field. J Comput Chem. 2005; 26:1452–1463. [PubMed: 16088926]

MacKerell AD Jr, Bashford D, Bellott M, Dunbrack RL Jr, Evanseck JD, Field MJ, Fischer S, Gao J, Guo H, Ha S, Joseph-McCarthy D, Kuchnir L, Kuczera K, Lau FTK, Mattos C, Michnick S, Ngo T, Nguyen DT, Prodhom B, Reiher WE III, Roux B, Schlenkrich M, Smith JC, Stote R, Straub J, Watanabe M, Wiórkiewicz-Kuczera J, Yin D, Karplus M. An all-atom empirical potential for molecular modeling and dynamics studies of proteins. J Phys Chem B. 1998; 102:3586–3616.

Mackerell AD Jr, Feig M, Brooks CL III. Extending the treatment of backbone energetics in protein force fields: limitations of gas-phase quantum mechanics in reproducing protein conformational distributions in molecular dynamics simulations. J Comput Chem. 2003; 25:1400–1415. [PubMed: 15185334]

Magotti P, Ricklin D, Qu H, Wu YQ, Kaznessis YN, Lambris JD. Structure-kinetic relationship analysis of the therapeutic complement inhibitor compstatin. Journal of molecular recognition : JMR. 2009; 22:495–505. [PubMed: 19658192]

Mallik B, Katragadda M, Spruce LA, Carafides C, Tsokos CG, Morikis D, Lambris JD. Design and NMR characterization of active analogues of compstatin containing non-natural amino acids. J Med Chem. 2005; 48:274–286. [PubMed: 15634022]

Mallik B, Lambris JD, Morikis D. Conformational inter-conversion of compstatin probed with molecular dynamics simulations. Proteins. 2003; 53:130–141. [PubMed: 12945056]

Mallik B, Morikis D. Development of a quasi-dynamic pharmacophore model for anticomplement peptide analogues. J Am Chem Soc. 2005; 127:10967–10976. [PubMed: 16076203]

Maminishkis A, Chen S, Jalickee S, Banzon T, Shi G, Wang FE, Ehalt T, Hammer JA, Miller SS. Confluent monolayers of cultured human fetal retinal pigment epithelium exhibit morphology and physiology of native tissue. Investigative ophthalmology & visual science. 2006; 47:3612–3624. [PubMed: 16877436]

Marmorstein RQ, Joachimiak A, Sprinzl M, Singler PB. The Structural Basis for the Interaction between L-Tryptophan and the Escherichia coli trp Aporepressor. J Biol Chem. 1987; 262:4922–4927. [PubMed: 3549712]

Morikis D, Assa-Munt N, Sahu A, Lambris JD. Solution structure of compstatin, a pontent complement inhibitor. Protein Sci. 1998; 7:619–627. [PubMed: 9541394]

Morikis D, Floudas CA, Lambris JD. Structure-based integrative computational and experimental approach for the optimization of drug design. Computational Science - Iccs. 2005; 2005(Pt 2): 680–688.

Morikis D, Lambris JD. Structural aspects and design of low molecular mass complement inhibitors. Biochem Soc T. 2002; 30:1026–1036.

Morikis, D.; Lambris, JD. Structure, dynamics, activity, and function of compstatin and design of more potent analogues. 6000 Broken Sound Parkway Nw, Ste 300, Boca Raton, Fl 33487-2742 USA: Crc Press-Taylor & Francis Group; 2005.

Morikis D, Roy M, Sahu A, Troganis A, Jennings PA, Tsokos GC, Lambris JD. The structural basis of compstatin activity examined by structure-function-based design of peptide analogs and NMR. J Biol Chem. 2002; 277:14942–14953. [PubMed: 11847226]

Morikis D, Soulika AM, Mallik B, Klepeis JL, Floudas CA, Lambris JD. Improvement of the anti-C3 activity of compstatin using rational and combinatorial approaches. Biochem Soc T. 2004; 32:28–32.

Qu H, Ricklin D, Bai H, Chen H, Reis ES, Maciejewski M, Tzekou A, DeAngelis RA, Resuello RRG, Lupu F, Barlow PN, Lambris JD. New analogs of the clinical complement inhibitor compstatin with subnanomolar affinity and enhanced pharmacokinetic properties. Immunobiology. 2013; 218:496–505. [PubMed: 22795972]

Qu H, Ricklin D, Lambris JD. Recent developments in low molecular weight complement inhibitors. Molecular Immunology. 2009; 47:185–195. [PubMed: 19800693]

Ricklin D, Lambris JD. Complement-targeted therapeutics. Nature Biotechnology. 2007; 25:1265–1275.

Ricklin D, Lambris JD. Compstatin: a complement inhibitor on its way to clinical application. Advances in experimental medicine and biology. 2008; 632:273–292. [PubMed: 19025129]

Rudolf M, Clark ME, Chimento MF, Li CM, Medeiros NE, Curcio CA. Prevalence and morphology of druse types in the macula and periphery of eyes with age-related maculopathy. Investigative ophthalmology & visual science. 2008; 49:1200–1209. [PubMed: 18326750]

Sahu A, Kay BK, Lambris JD. Inhibition of human complement by a C3 binding peptide isolated from a phage displayed random peptide library. J Immunol. 1996; 157:884–891. [PubMed: 8752942]

Sahu A, Morikis D, Lambris JD. Compstatin, a peptide inhibitor of complement, exhibits species-specific binding to complement component C3. Mol Immunol. 2003; 39:557–566. [PubMed: 12431389]

Sahu A, Soulika AM, Morikis D, Spruce L, Moore WT, Lambris JD. Binding Kinetics, Structure-Activity Relationship, and Biotransformation of the Complement Inhibitor Compstatin. J Immunol. 2000; 165:2491–2499. [PubMed: 10946275]

Song MK, Kim SY, Lee J. Understanding the structural characteristics of compstatin by conformational space annealing. Biophysical Chemistry. 2005; 115:201–207. [PubMed: 15752605]

Soulika AM, Morikis D, Sarrias MR, Roy M, Spruce LA, Sahu A, Lambris JD. Studies of structure-activity relations of complement inhibitor compstatin. J Immunol. 2003; 171:1881–1890. [PubMed: 12902490]

Tamamis P, López de Victoria A, Gorham RD Jr, Bellows-Peterson ML, Pierou P, Floudas CA, Morikis D, Archontis G. Molecular dynamics in drug design: new generations of compstatin analogs. Chem Biol Drug Des. 2012; 79:703–718. [PubMed: 22233517]

Tamamis P, Morikis D, Floudas CA, Archontis G. Species specificity of the complement inhibitor compstatin investigated by all-atom molecular dynamics simulations. Proteins. 2010; 78:2655–2667. [PubMed: 20589629]

Tamamis P, Pierou P, Mytidou C, Floudas CA, Morikis D, Archontis G. Design of a modified mouse protein with ligand binding properties of its human analog by molecular dynamics simulations: The case of C3 inhibition by compstatin. Proteins. 2011; 79:3166–3179. [PubMed: 21989937]

Tamamis P, Skourtis SS, Morikis D, Lambris JD, Archontis G. Conformational analysis of compstatin analogues with molecular dynamics simulations in explicit water. J Mol Graph Model. 2007; 26:571–580. [PubMed: 17498990]

Valkó K. Application of high-performance liquid chromatography based measurements of lipophilicity to model biological distribution. Journal of chromatography A. 2004; 1037:299–310. [PubMed: 15214672]

Yehoshua Z, Rosenfeld PJ, Albini TA. Current Clinical Trials in Dry AMD and the Definition of Appropriate Clinical Outcome Measures. Semin. Ophthalmol. 2011; 26:167–180. [PubMed: 21609230]

Yesselman JD, Price DJ, Knight JL, Brooks CL III. MATCH: An Atom-Typing Toolset for Molecular Mechanics Force Fields. Journal of Computational Chemistry. 2012; 33:189–202. [PubMed: 22042689]

Zarbin MA, Rosenfeld PJ. PATHWAY-BASED THERAPIES FOR AGE-RELATED MACULAR DEGENERATION An Integrated Survey of Emerging Treatment Alternatives. Retina-the Journal of Retinal and Vitreous Diseases. 2010; 30:1350–1367.

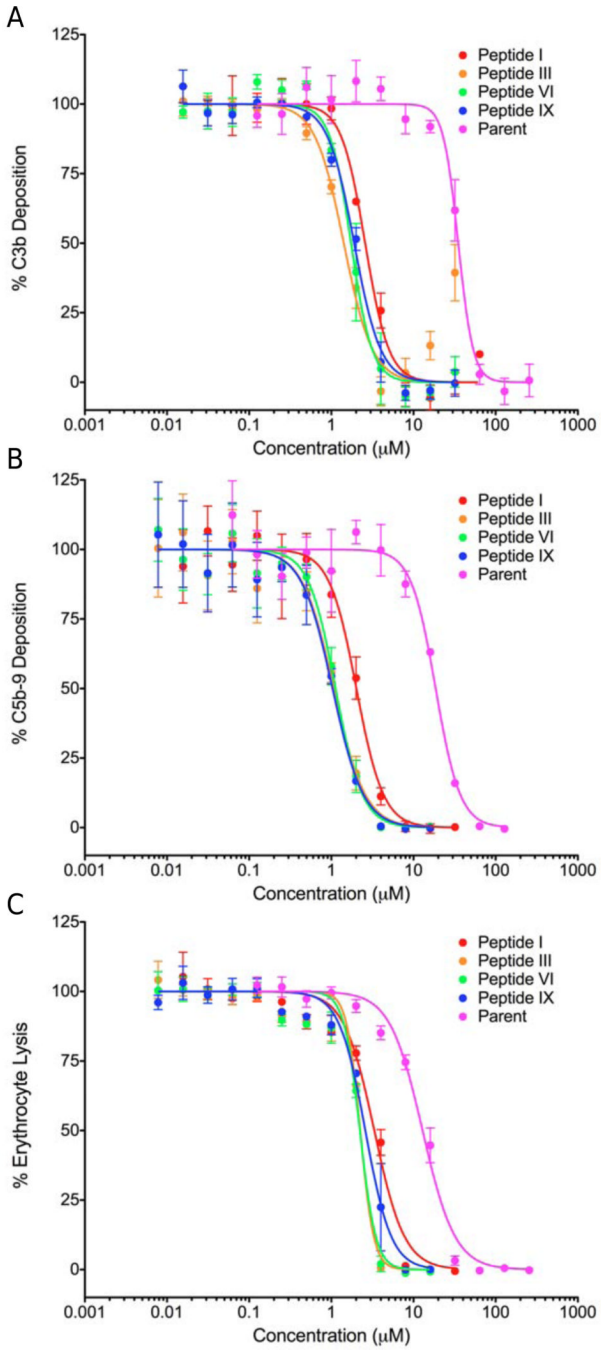

Figure 1. ELISA and hemolytic assay data used to extract the IC_{50} values of Table 1

(A) C3b ELISA data, representing the inhibition of cleavage of C3 to C3a and C3b by compstatin peptides, quantified as inhibition of the formation of C3b. (B) C5b-9 ELISA data, representing inhibition of the 7formation of the C5b-9 terminal complex of complement activation. (C) Hemolytic assay data, representing inhibition of rabbit erythrocyte hemolysis by the C5b-9 terminal complex activation. The data points and error bars correspond to means and S.E.M. from three independent experiments.

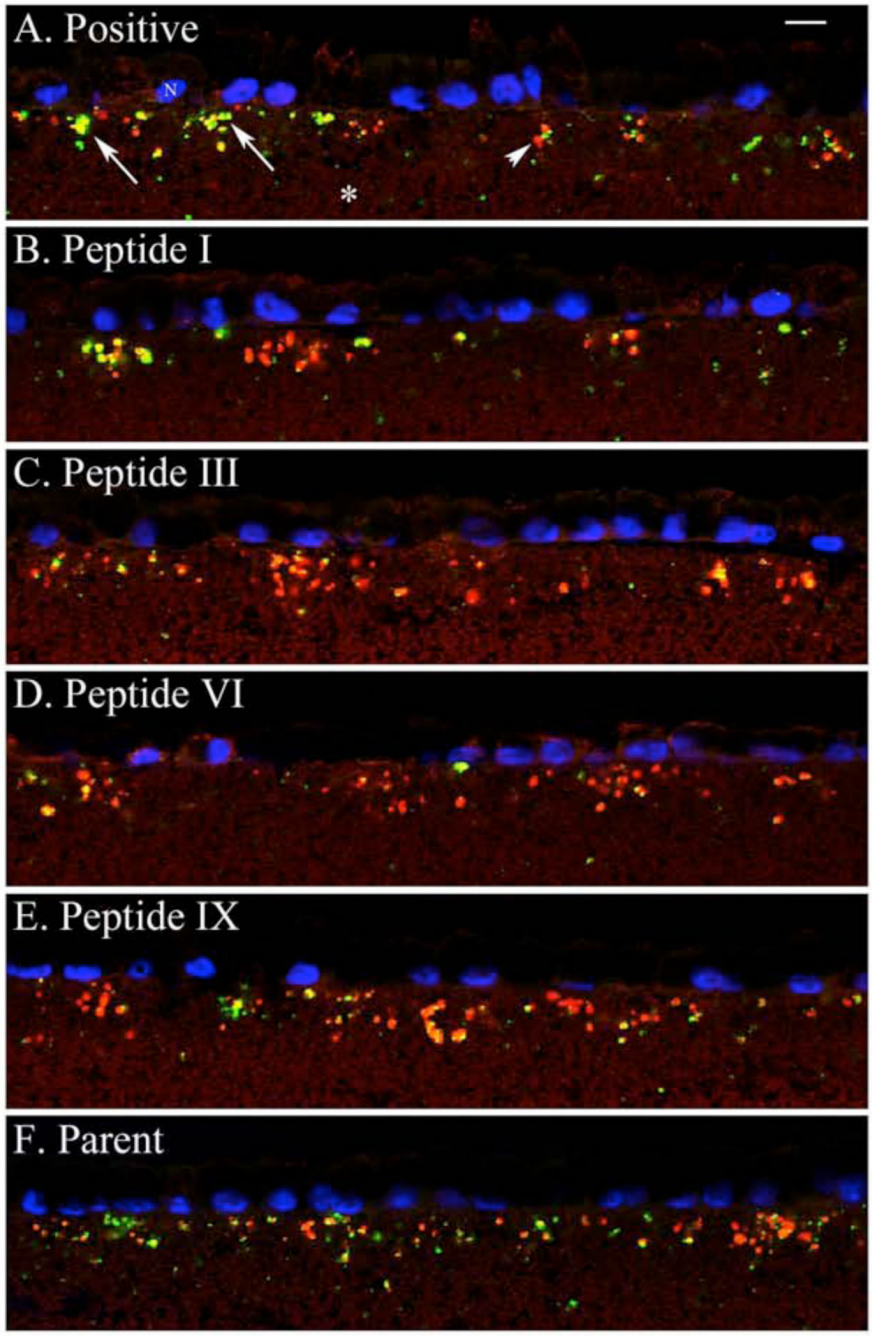

Figure 2. Confocal microscopy immunofluorescence images of C5b-9 deposition

Examples of confocal immunofluorescence images of sub-RPE deposit-associated C5b-9 immunolabeling (green). ApoE immunolabeling of deposits is in red, with areas of co-localization represented by yellow fluorescence. The effects of the inhibitory peptides are illustrated by the reduced amounts of green C5b-9-specific labeling in B-F. Consistent with the C5b-9 ELISA data, Peptides III, VI, and IX reduce C5b-9-specific labeling most significantly compared to the positive control (A). N = nucleus (blue) in A; arrows in A indicate C5b-9 immunolabeling (green); arrowhead in A indicates ApoE deposits (red); red background autofluorescence of the cell culture support is indicated by asterisk in A; scale bar in A = 10 μm.

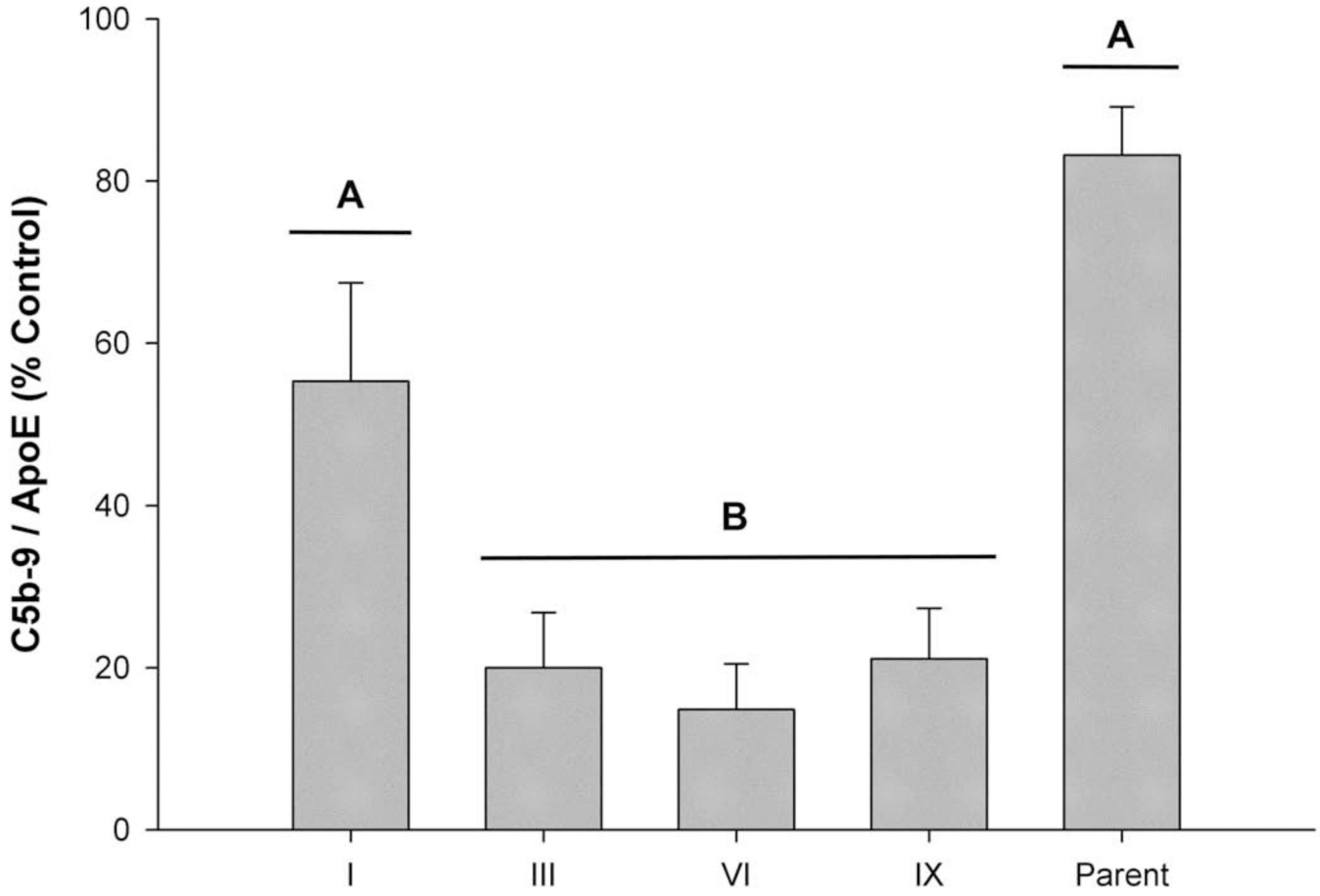

Figure 3. Confocal analysis of C5b-9 deposition

The ratio of deposit-associated C5b-9 fluorescence, a variable measure of complement activation, to ApoE fluorescence, a relatively constant deposit marker, is shown relative to the positive (human serum only) control. All peptides, except for the parent compound, significantly decrease complement activation. Although Peptide I decreases complement activation compared to the parent compound (group A), the difference is not statistically significant. Peptides III, VI, and IX (group B) are the most effective, and are all significantly different ($p < 0.001$) from the parent compound and from peptide I. Bars represent the means (± S.E.M.) of the combined data from RPE cultures derived from three different donors.

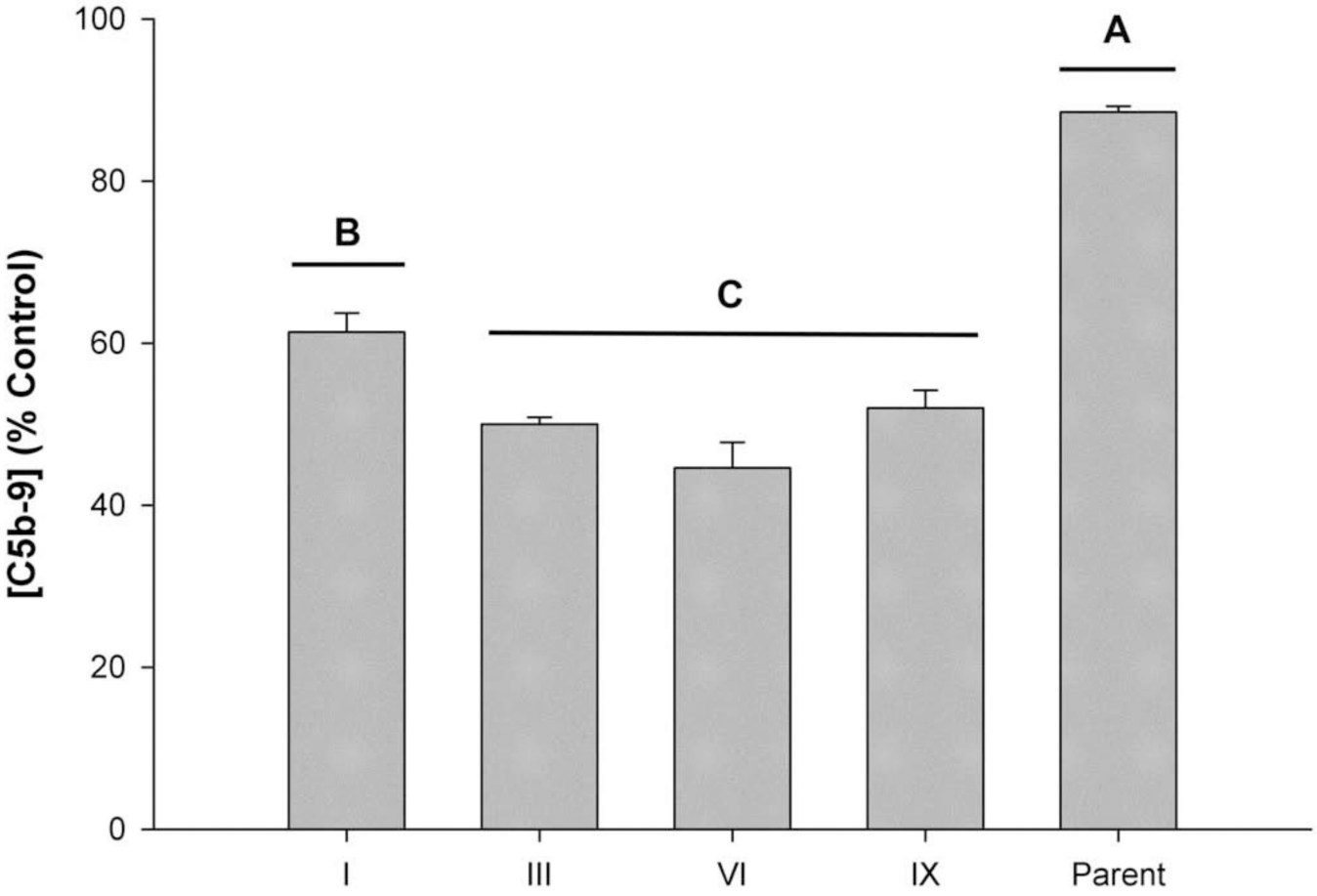

Figure 4. C5b-9 ELISA

Relative to the positive control, all inhibitory peptides significantly decrease the amount of soluble C5b-9 present in the assay medium. Peptide I (B) is more effective than the parent peptide (A), but less inhibitory than peptides III, VI, and IX (group C) which are the most effective inhibitors and are all significantly different ($p < 0.001$) from the parent peptide and peptide I (A and B). Bars represent the means (± S.E.M.) of the combined data from RPE cultures derived from three different donors.

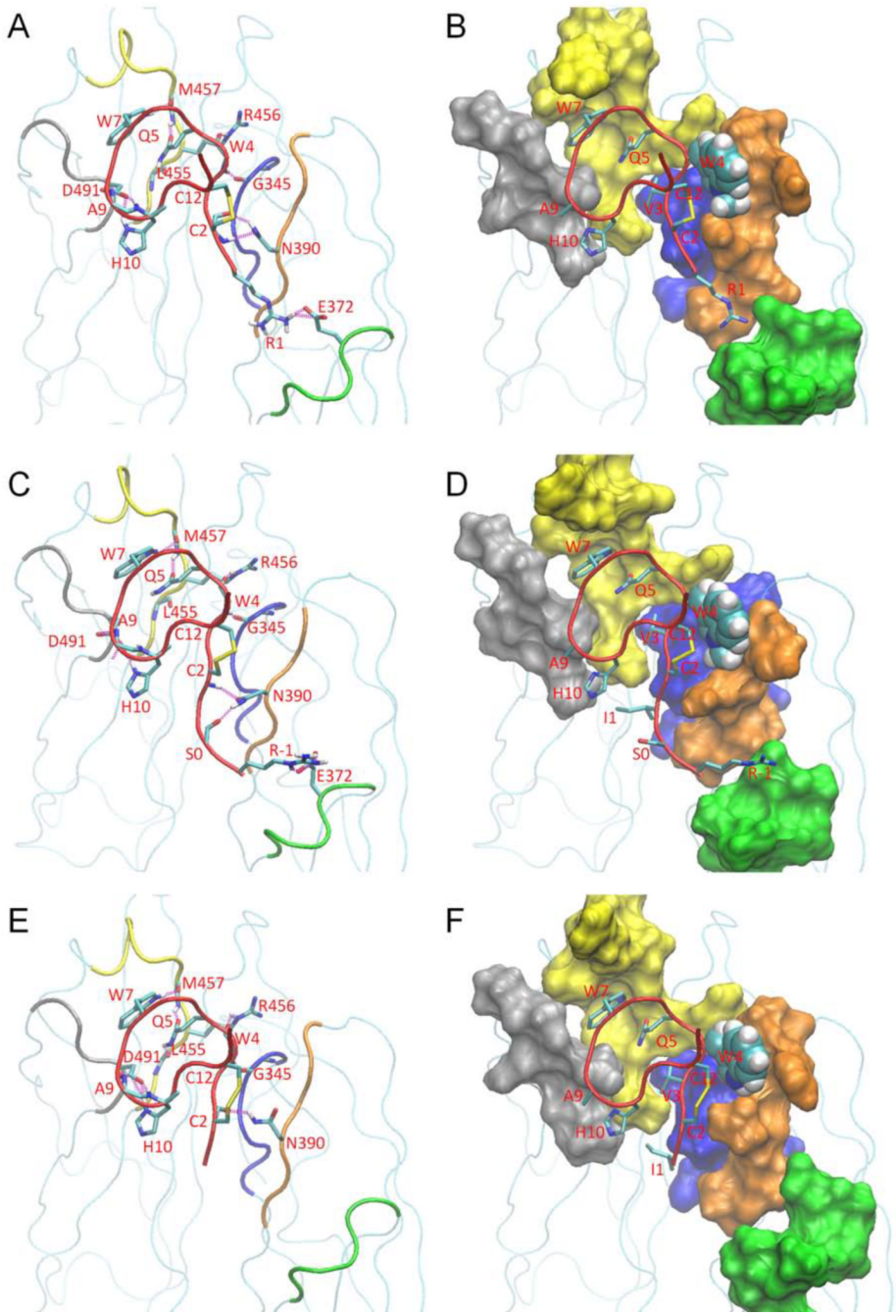

Figure 5. Intermolecular contacts of Peptides III, VI and IX with C3 from molecular dynamics simulations

Simulation structures of the C3 binding site with Peptides III (A, B), VI (C, D), and control Peptide IX (E, F) (Tamamis et al., 2010; Tamamis et al., 2012) at the end of the molecular dynamics simulations. Important hydrogen bonds and nonpolar binding pockets are shown, respectively, in the left and right panels. Five interacting C3 sectors (344–349; orange, 371–376; green, 388–393; blue, 454–462; yellow and 488–492; gray) with heavy atoms up to 7.5 Å from the Peptide VI ligand are shown in tube (A, C, E) and surface (B, D, F) representation. The purple lines in (A, C, E) denote important hydrogen bonds. All hydrogen atoms, except for those participating in hydrogen bonds (in A, C, E), are omitted for clarity.

In panels (A, C, E) important main/side chain hydrogen bonding protein-ligand residue pairs are shown in licorice. In panels (B, D, F) important ligand side chain groups, lying on or binding into the protein surface, are shown in licorice.

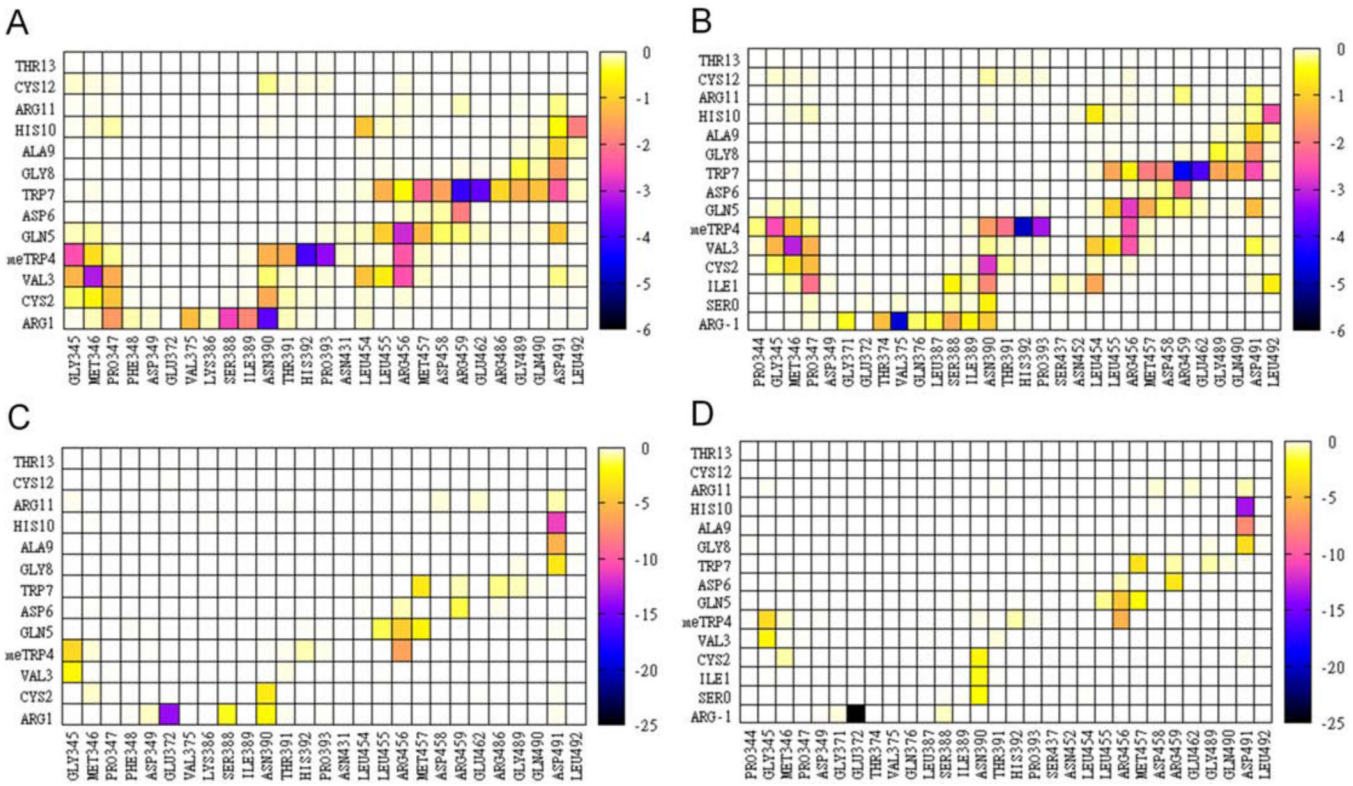

Figure 6. Energetic analysis of intermolecular contacts of Peptides III and VI with C3 from molecular dynamics simulations

Two dimensional density maps depicting the favorable (negative) average MM GBSA interaction free-energies for intermolecular ligand (y axis) – C3 (x axis) interacting residue pairs, within the simulation of Peptides III (A, C) and VI (B, D) in complex with C3. The upper panels (A, B) correspond to polar interactions, and the bottom panels (B, D) correspond to nonpolar interactions. All energies are in kcal/mol. The color code for the interaction free energy is shown in the palette on the right-hand side of each panel.

Table 1

Compstatin peptide sequences.

Peptide	Sequence[a]	Molecular Mass[b]
	N-terminus modification analogs	
	-10 123 4567890123[c]	
I	Ac- **R**CV WQDWGAHRCT-NH_2	1656.0
II	Ac- **meW**CV WQDWGAHRCT-NH_2	1700.4
III	Ac- **R**CV**meW**QDWGAHRCT-NH_2	1669.8
	N-terminus extension analogs	
IV	Ac-**SS**-ICV WQDWGAHRCT-NH_2	1787.7
V	Ac-**WW**-**R**CV WQDWGAHRCT-NH_2	2029.0
VI	Ac-**RS**-ICV**meW**QDWGAHRCT-NH_2	1870.6
VII	Ac-**RS**-**R**CV**meW**QDWGAHRCT-NH_2	1913.4
VIII	Ac-**SS**-**R**CV**meW**QDWGAHRCT-NH_2	1844.3
	Control analogs	
IX	Ac- ICV WQDWGAHRCT-NH_2	1614.0
Parent	ICV VQDWGHHRCT-NH_2	1549.8

[a] Bold face characters denote new amino acid combinations. Tryptophans methylated at the indole amide position are shown as meW. The peptides are cyclized with a disulfide bridge between C2 and C12. Ac denotes acetylation and NH_2 denotes amidation.

[b] From mass spectrometry.

[c] Numbering indicates sequence position, starting from position −1 and ending at position 13.

Table 2

Compstatin peptide IC_{50} values from C3b and C5b-9 ELISA, and hemolytic assay.

Peptide	IC_{50} (μM)[a]	95% confidence interval
C3b ELISA		
I	2.58	2.27–2.94
III	1.42	1.14–1.77
VI	1.74	1.50–2.02
IX	1.90	1.71–2.10
Parent	35.04	31.26–39.29
C5b-9 ELISA		
I	2.02	1.66–2.46
III	1.07	0.85–1.36
VI	1.13	0.94–1.34
IX	1.04	0.80–1.33
Parent	18.61	15.65–22.14
Hemolytic assay		
I	3.33	2.99–3.72
III	2.25	2.08–2.43
VI	2.23	2.05–2.42
IX	2.59	2.28–2.95
Parent	12.90	11.71–14.21

[a]Means from three independent experiments.

Table 3

Compstatin peptide inhibition from the RPE cell-based assay data.

Peptide	Confocal Imaging % of positive control	Assay medium C5b-9 ELISA % of positive control
I	55.27 (12.30)[a]	61.37 (2.34)[a]
III	19.98 (6.84)	50.02 (0.82)
VI	14.85 (5.61)	44.60 (3.16)
Controls		
IX	21.11 (6.26)	51.99 (2.21)
Parent	83.19 (5.92)	88.49 (0.76)
Negative (no human serum)	0.34 (0.30)	2.62 (0.79)
Positive (human serum)	100	100

[a]Mean (S.E.M.).

Table 4

Chromatographic parameters of compstatin peptides in the order of increasing lipophilicity.

Peptide	Peptide Sequence	No. of Charges[a]	No. of W	t_R[b] (min)	k[c]	log$k$
Parent	ICV VQDWGHHRCT-NH_2	2+[d], 1−, 2H	1W	4.995±0.003	2.472±0.006	0.393
I	Ac- RCV WQDWGAHRCT-NH_2	2+, 1−, 1H	2W	5.507±0.014	2.828±0.012	0.451
III	Ac- RCVmeWQDWGAHRCT-NH_2	2+, 1−, 1H	1W, 1meW	10.307±0.023	6.165±0.021	0.790
VI	Ac-RS-ICVmeWQDWGAHRCT-NH_2	2+, 1−, 1H	1W, 1meW	15.700±0.022	9.913±0.026	0.996
IX	Ac- ICV WQDWGAHRCT-NH_2	1+, 1−, 1H	2W	17.880±0.028	11.429±0.031	1.058

[a] The number of histidines (marked with H) is included, because they may be positively charged or neutral, depending on their pK_a values.

[b] Retention time.

[c] Retention factor *(k)*.

[d] Includes positive charge of the unblocked backbone of the N-terminus.

Table 5

Intermolecular hydrogen-bond occupancies for Peptides III and VI in complex with C3, from the analysis of molecular dynamics trajectories.

Intermolecular Atom Pairs		Hydrogen Bond Occupancy (%) Peptide III	Hydrogen Bond Occupancy (%) Peptide VI
Arg-1 Side-NH1/2	Asn371 Main-O	-	21
Arg-1 Side-NH1/2	Glu372 Side-OE1/2	-	100
Arg-1 Side-NE	Glu372 Side-OE1/2	-	98
Ser0 Main-O	Asn390 Side-ND2	-	77
Ile/Arg1 Side-NH1/2	Glu372 Side-OE1/2	77	-
Ile/Arg1 Side-NE	Glu372 Side-OE1/2	33	-
Arg1 Side-NH1/2	Ser388 Main-O	37	-
Cys2 Main-N	Asn390 Side-OD1	76	91
Cys2 Main-N	Asn390 Side-ND2	9	12
Cys2 Main-O	Asn390 Side-ND2	50	-
Trp4 Main-O	Arg456 Side-NH1/2	52	52
Trp4 Main-O	Arg456 Side-NE	97	96
Trp4 Main-N	Gly345 Main-O	100	100
Gln5 Side-OE1	Met457 Main-N	96	95
Gln5 Side-NE2	Leu455 Main-O	64	57
Asp6 Main-O	Arg459 Side NH1/2	4	12
Trp7 Side-NE1	Met457 Main-O	96	99
Ala9 Main-N	Asp491 Side-OD1/2	88	100
His10 Side-N	Asp491 Side-OD1/2	74	91
His10 Main-ND1	Asp491 Side-OD1/2	79	100

Percent occupancies have been computed from the analysis of 140/200 snapshots (per trajectory), extracted at 50-ps intervals from the five 7/10-ns molecular dynamics trajectories, respectively for Peptides III/VI. A hydrogen bond was present if the donor (D) – acceptor (A) distance was less than 3.5 Å and the corresponding angle (D-H⋯ A) was larger than 90°. “Main“ and “Side” refer to main chain and side chain donors/acceptors.